# Interband Magneto-Absorption and Faraday Rotation in InSb

C. R. PIDGEON AND R. N. BROWN*
*National Magnet Laboratory,† Massachusetts Institute of Technology, Cambridge, Massachusetts*
(Received 24 January 1966)

Direct interband magneto-optical transitions have been observed in pure $n$-type InSb at liquid-helium temperature using magnetic fields up to 96.5 kG. The theory of the magnetic levels in the valence and conduction bands at the zone center is carried out using a modification of the method of Luttinger and Kohn. The interaction between conduction and valence bands has been treated exactly, and the effect of higher bands to order $k^2$. Selection rules have been evaluated for both allowed ($\Delta n=0, -2$) and warping-induced ($\Delta n=2, \pm 4, -6$) direct valence-to-conduction-band transitions. Comparison of theoretical with experimental spectra (using circular and plane-polarized light in the Faraday and Voigt configurations, respectively) has shown good agreement for the magnetic field in the [110] and [100] crystal directions. The following band parameters are obtained: conduction-band effective mass $m_c=0.0145\ m_0$: light-hole effective mass $m_{l.h.}=0.0160\ m_0$; heavy-hole effective masses $m_{h.h.}[100]=0.32\ m_0$, $m_{h.h.}[110]=0.42\ m_0$, $m_{h.h.}[111]=0.44\ m_0$.

## INTRODUCTION

SINCE the observation of the interband magneto-optical effect in InSb by Burstein *et al.*, and Zwerdling *et al.*,[1] various workers have investigated the phenomenon in this material. Interband magneto-reflection has been studied by Wright and Lax,[2] and a more detailed investigation of magneto-absorption in InSb has been made by Zwerdling *et al.*[3] The phenomenon has also been observed at low fields in Faraday rotation by Smith *et al.*[4] Further measurements of magneto-absorption and Faraday rotation were given recently by Pidgeon and Brown.[5] As has been pointed out by Dresselhaus,[6] previous analyses have been most appropriate in the high-quantum (classical) limit. A discussion of the fine structure in the low-quantum limit has not been given. Further, the preliminary band-parameter constants obtained from an analysis of the heavy-hole anisotropy in the classical region[3] differed from those obtained by Bagguley *et al.*[7] in a recent cyclotron-resonance experiment.

In this paper we present high-field measurements of interband magneto-absorption in InSb at liquid-helium temperature for both the Faraday and Voigt configurations using circular and plane-polarized light, respectively. Further results are given for the interband Faraday rotation.

The theory of the magnetic energy levels in the valence and conduction bands at the zone center is carried out using a modification of the effective-mass method of Luttinger and Kohn (L.K.).[8] Following Kane's[9] treatment of the zero-field case, we have included the coupling between the conduction and valence bands exactly, and the effect of higher bands to order $k^2$. The approach is similar to the intra-band study of Bowers and Yafet.[10] Thus, the effects of non-parabolic conduction and light-hole bands, warping of the conduction and valence bands, and the "quantum effects" of the light and heavy-hole valence bands are included.

Selection rules are evaluated for both allowed and forbidden direct (valence-to-conduction-band) transitions at $\mathbf{k}=0$. The dominant allowed transitions obey the selection rules $\Delta n=0, -2$ where $n$ is the Landau orbital quantum number. In addition there is a further set of allowed transitions resulting from the inclusion of the full anisotropy in the effective-mass Hamiltonian according to the method of Luttinger.[11] These transitions are associated with the warping-induced harmonics observed in cyclotron resonance in Ge at 1.5°K (Hensel,[12] Stickler *et al.*[13]). Forbidden transitions may also arise in InSb because of the lack of inversion symmetry (see Elliott *et al.*,[14] Burstein *et al.*,[15] Roth *et al.*[16]). The dominant forbidden transitions arise from the first-

* Present address: Schlumberger Well Surveying Corporation, Ridgefield, Connecticut.

† Supported by the U. S. Air Force Office of Scientific Research.

[1] E. Burstein, G. S. Picus, and H. A. Gebbie, Phys. Rev. **103**, 825 (1956); S. Zwerdling, B. Lax, and L. M. Roth, Phys. Rev. **108**, 1402 (1957).

[2] G. B. Wright and B. Lax, J. Appl. Phys. (Suppl.) **32**, 2113 (1961).

[3] S. Zwerdling, W. H. Kleiner, and J. P. Theriault, J. Appl. Phys. Suppl. **32**, 2118 (1961); in *Proceedings of the International Conference on the Physics of Semiconductors, Exeter* (The Institute of Physics and the Physical Society, London, 1962), p. 455.

[4] S. D. Smith, C. R. Pidgeon, and V. Prosser in *Proceedings of the International Conference on the Physics of Semiconductors, Exeter* (The Institute of Physics and the Physical Society, London, 1962), p. 301; I. M. Boswarva, Proc. Phys. Soc. (London) **84**, 389 (1964).

[5] C. R. Pidgeon and R. N. Brown, Bull. Am. Phys. Soc. **11**, 52 (1966).

[6] G. Dresselhaus, Proceedings of the Varenna Summer School on Physics of Semiconductors, 1965 (to be published).

[7] D. M. S. Bagguley, M. L. A. Robinson, and R. A. Stradling, Phys. Letters **6**, 143 (1963).

[8] J. M. Luttinger and W. Kohn, Phys. Rev. **97**, 869 (1955).

[9] E. O. Kane, J. Phys. Chem. Solids **1**, 249 (1957).

[10] R. Bowers and Y. Yafet, Phys. Rev. **115**, 1165 (1959).

[11] J. M. Luttinger, Phys. Rev. **102**, 1030 (1956).

[12] J. C. Hensel, in *Proceedings of the International Conference on the Physics of Semiconductors, Exeter* (The Institute of Physics and the Physical Society, London, 1962), p. 281.

[13] J. J. Stickler, H. J. Zeiger, and G. S. Heller, Phys. Rev. **127**, 1077 (1962).

[14] R. J. Elliott, T. P. McLean, and G. C. MacFarlaine, Proc. Phys. Soc. (London) **72**, 553 (1958).

[15] E. Burstein, G. S. Picus, R. F. Wallis, and F. Blatt, Phys Rev. **113**, 15 (1959).

[16] L. M. Roth, B. Lax, and S. Zwerdling, Phys. Rev. **114**, 90 (1959).

order term in the wave function and obey the selection rules $\Delta n=\pm 1$. Linear $-\mathbf{k}$ terms may also give rise to forbidden transitions (Dresselhaus[17]) but these are expected to be extremely weak (Kane[9]) and are neglected in the present work.

In the first section we give the theory for the energy levels of the valence and conduction bands in a magnetic field. The solutions are computed from two 4×4 numerical matrices for a given set of conduction and valence-band parameters, with the magnetic-field direction in the $(1\bar{1}0)$ plane. The selection rules and transition probabilities are evaluated in the second section for left and right circularly polarized light in the Faraday configuration ($\sigma_L$ and $\sigma_R$) and for plane polarized light with the electric vector parallel to the applied magnetic field ($\mathbf{E}\|\mathbf{H}$) in the Voigt configuration ($\pi$ spectrum). In the third section we present the experimental methods and results for thin freely mounted samples of pure $n$-type InSb at liquid helium temperature, using magnetic fields up to 96.5 kG. Finally the theoretical and experimental spectra are compared and the band parameters successively adjusted to give the best over-all fit. An attempt is made to interpret the spectral fine structure in the low-quantum-number region in terms of additional transitions resulting from the anisotropy of the valence bands.

## THEORY

### I. Energy Levels in a Magnetic Field

In this section we obtain the energy levels according to the L.K. method with the modification that we treat the conduction band together with the degenerate valence band set. We work in a right-handed coordinate system defined by (1,2,3) and assume the applied magnetic field $H$ is in the 3 direction. The energy levels are the eigenvalues of the following set of coupled equations (we work throughout in atomic units):

$$\sum_{j'}\{D_{jj'}{}^{\alpha\beta}k_\alpha k_\beta+\pi_{jj'}{}^{\alpha}k_\alpha +\tfrac{1}{2}s(\sigma_3)_{jj'}+(1/4c^2)[(\boldsymbol{\sigma}\times\boldsymbol{\nabla}V)\cdot\mathbf{p}]_{jj'} +\epsilon_{j'}\delta_{jj'}\}f_{j'}(\mathbf{r})=\epsilon f_j(\mathbf{r}), \quad (1)$$

where

$$D_{jj'}{}^{\alpha\beta}\equiv\tfrac{1}{2}\delta_{jj'}\delta_{\alpha\beta}+\sum_i[\pi_{ji}{}^{\alpha}\pi_{ij'}{}^{\beta}/(\epsilon_0'-\epsilon_i)], \quad (2)$$

$j$ and $j'$ run over the two conduction- and six valence-band states, $i$ runs over all higher bands, and $\alpha/\beta$ run over 1, 2, and 3. $\epsilon_i$ is the energy of the $i$th state; $\epsilon_0$ represents an average energy for the set of states $j$. The quantity $\pi_{jj'}$ is the modified momentum matrix element between bands $j$ and $j'$ at $\mathbf{k}=0$ which includes spin-orbit interaction:

$$\pi_{jj'}=\int u_{j,0}{}^*(\mathbf{r})\left[\mathbf{p}-\frac{1}{4c^2}(\boldsymbol{\nabla}V\times\boldsymbol{\sigma})\right]u_{j',0}(\mathbf{r})d\mathbf{r}, \quad (3)$$

where $u_{j,0}(\mathbf{r})$ is the Bloch function at $\mathbf{k}=0$ for the $j$th band, $V$ is the crystal potential, $\sigma$ the Pauli spin matrix, and $c$ the velocity of light. Following Kane[9] and Roth,[16] we neglect contributions from the second term in $\pi_{jj'}$. We define the operator $\mathbf{k}=(\mathbf{p}+e\mathbf{A}/c)$, where $\mathbf{p}$ is the momentum, $e$ the proton charge, and $\mathbf{A}$ the vector potential of the applied magnetic field. We use the Landau gauge $\mathbf{A}=H(-x_2,0,0)$ where the position vector $\mathbf{r}=(x_1,x_2,x_3)$ in the (1,2,3) coordinate system, and $s=eH/c$. The functions $f_j(\mathbf{r})$ are envelope functions, and the total zeroth-order wave function is given by

$$\Psi(\mathbf{r})=\textstyle\sum_j f_j(\mathbf{r})u_{j,0}(\mathbf{r}). \quad (4)$$

The second term in Eq. (1) represents the interaction between the conduction and valence bands which reduces to Kane's $\mathbf{k}\cdot\mathbf{p}$ interaction term in zero field. The third term is the spin magnetic energy and the fourth term is the contribution of the spin-orbit coupling. We have neglected a small additional contribution in Eq. (1) arising from interband matrix elements of the spin-orbit interaction. As shown by (L.K.) the correct zero-order wave functions in the $(x,y,z)$ crystal coordinate system are

$$\begin{aligned}
&u_{1,0}(\mathbf{r})=|S\uparrow\rangle;\quad u_{2,0}(\mathbf{r})=|iS\downarrow\rangle;\\
&u_{3,0}(\mathbf{r})=|(1/\sqrt{2})(X+iY)\uparrow\rangle;\\
&u_{4,0}(\mathbf{r})=|(i/\sqrt{2})(X-iY)\downarrow\rangle; \quad (5)\\
&u_{5,0}(\mathbf{r})=|(1/\sqrt{6})[(X-iY)\uparrow+2Z\downarrow]\rangle;\\
&u_{6,0}(\mathbf{r})=|(i/\sqrt{6})[(X+iY)\downarrow-2Z\uparrow]\rangle;
\end{aligned}$$

$$\begin{aligned}
&u_{7,0}(\mathbf{r})=|(i/\sqrt{3})[-X-iY)\uparrow+Z\downarrow]\rangle;\\
&u_{8,0}(\mathbf{r})=|(1/\sqrt{3})[(X+\mathrm{i}Y)\downarrow+Z\uparrow]\rangle; \quad (6)
\end{aligned}$$

where the symbol $\uparrow$ means spin up and $\downarrow$ means spin down. $S$ is the conduction-band function which transforms as an atomic $s$ function; $X$, $Y$, $Z$ are the valence-band functions which transform as atomic $p$ functions under the operations of the tetrahedral group at the point $\Gamma$.

The effective-mass Hamiltonian may now be written as an 8×8 matrix $D$. Following Luttinger we assume $\mathbf{H}$ is in the $(1\bar{1}0)$ plane, and write $D$ in two parts:

$$D=D_0+D_1, \quad (7)$$

where part of the anisotropy is included in $D_0$ which can be solved exactly. The other part in $D_1$ is treated by second-order perturbation theory in Appendix A. We make the approximation $k_3=0$, which has been justified by Goodman[18] for the case of Ge. $D_0$ may be written in terms of two 4×4 matrices:

$$D_0=\left|\left|\begin{matrix}D_a & 0\\ 0 & D_b\end{matrix}\right|\right|, \quad (8)$$

[17] G. Dresselhaus, Phys. Rev. **100**, 580 (1955).

[18] R. R. Goodman, Phys. Rev. **122**, 397 (1961).

apart from matrix elements of type (Kane[9]):

$$G=\sum_i\langle S|p_x|i\rangle\langle i|p_y|Z\rangle/(\epsilon_0-\epsilon_i), \tag{9}$$

which appear in the off-diagonal blocks. This term is nonzero because of the lack of inversion symmetry. However, since $G$ is estimated to be of the order of 2 (Bowers and Yafet[10]), its effect on the energy levels will be small compared to that of the elements in $D_a$ and $D_b$, and therefore we neglect it. We then have the following eigenvalue equations in matrix form:

$$(D_a-\epsilon_a 1)f_a=0;\quad (D_b-\epsilon_b 1)f_b=0.$$

We write these explicitly:

$$\begin{bmatrix} 2sF(N+\frac{1}{2})+\epsilon_g-\epsilon_a+s(N+1) & i(s)^{1/2}Pa^\dagger & i(\frac{1}{3}s)^{1/2}Pa & (\frac{2}{3}s)^{1/2}Pa \\ -i(s)^{1/2}Pa & -s[(\gamma+\gamma')(N+\frac{1}{2})+\frac{3}{2}\kappa]-\epsilon_a & -s(3)^{1/2}\gamma''a^2 & -is(6)^{1/2}\gamma'a^2 \\ -i(\frac{1}{3}s)^{1/2}Pa^\dagger & -s(3)^{1/2}\gamma''a^{\dagger 2} & -s[(\gamma_1-\gamma')(N+\frac{1}{2})-\frac{1}{2}\kappa]-\epsilon_a & is(2)^{1/2}[\gamma'(N+\frac{1}{2})-\frac{1}{2}\kappa] \\ (\frac{2}{3}s)^{1/2}Pa^\dagger & is(6)^{1/2}\gamma'a^{\dagger 2} & -is(2)^{1/2}[\gamma'(N+\frac{1}{2})-\frac{1}{2}\kappa] & -s[\gamma_1(N+\frac{1}{2})-\kappa]-\Delta-\epsilon_a \end{bmatrix}\begin{bmatrix} f_1 \\ f_3 \\ f_5 \\ f_7 \end{bmatrix}=0, \tag{10}$$

and

$$\begin{bmatrix} \epsilon_g-\epsilon_b+2sF(N+\frac{1}{2})+sN & 2(\frac{1}{3}s)^{1/2}Pa^\dagger & i(s)^{1/2}Pa & (\frac{2}{3}s)^{1/2}Pa^\dagger \\ -i(\frac{1}{3}s)^{1/2}Pa & -s[(\gamma_1-\gamma')(N+\frac{1}{2})+\frac{1}{2}\kappa]-\epsilon_b & -s(3)^{1/2}\gamma''a^2 & is(2)^{1/2}[\gamma'(N+\frac{1}{2})+\frac{1}{2}\kappa] \\ -i(s)^{1/2}Pa^\dagger & -s(3)^{1/2}\gamma''a^{\dagger 2} & -s[(\gamma_1+\gamma')(N+\frac{1}{2})-\frac{3}{2}\kappa]-\epsilon_b & is(6)^{1/2}\gamma'a^{\dagger 2} \\ (\frac{2}{3}s)^{1/2}Pa & -is(2)^{1/2}[\gamma'(N+\frac{1}{2})+\frac{1}{2}\kappa] & -is(6)^{1/2}\gamma'a^2 & -s[\gamma_1(N+\frac{1}{2})+\kappa]-\Delta-\epsilon_b \end{bmatrix}\begin{bmatrix} f_2 \\ f_6 \\ f_4 \\ f_8 \end{bmatrix}=0. \tag{11}$$

Here we have introduced the creation and destruction operators $a$ and $a^\dagger$, where

$$\begin{aligned} a^\dagger&=(1/2s)^{1/2}(k_1+ik_2);\\ a&=(1/2s)^{1/2}(k_1-ik_2);\quad N=a^\dagger a. \end{aligned} \tag{12}$$

$P$ is the momentum matrix element defined by Kane ($P=-i\langle S|p_z|Z\rangle$); $\gamma'$ and $\gamma''$ are given by the following equations:

$$\begin{aligned} \gamma'&=\gamma_3+(\gamma_2-\gamma_3)[(3\cos^2\theta-1)/2]^2,\\ \gamma''&=\tfrac{2}{3}\gamma_3+\tfrac{1}{3}\gamma_2+\tfrac{1}{6}(\gamma_2-\gamma_3)[(3\cos^2\theta-1)/2]^2, \end{aligned} \tag{13}$$

where $\theta$ is the angle between the magnetic field and the $z$ axis. The valence-band parameters $\gamma_1$, $\gamma_2$, $\gamma_3$, and $\kappa$ are not those of Luttinger ($\gamma_1^L,\gamma_2^L,\gamma_3^L,\kappa^L$) since the contributions of the conduction band, which is treated exactly and not as a higher band, must be subtracted off. They are related to the Luttinger parameters by the following expressions:

$$\begin{aligned} \gamma_1&=\gamma_1^L-2P^2/3\epsilon_g,\\ \gamma_2&=\gamma_2^L-P^2/3\epsilon_g,\\ \gamma_3&=\gamma_3^L-P^2/3\epsilon_g,\\ \kappa&=\kappa^L-P^2/3\epsilon_g, \end{aligned} \tag{14}$$

where $\epsilon_g$ is the energy gap at $\mathbf{k}=0$. $\Delta$ is the spin-orbit splitting. $F$ is the conduction-band matrix element defined by Kane[9]:

$$F=\sum_i|\langle S|p_x|i\rangle|^2/(\epsilon_0-\epsilon_i). \tag{15}$$

By inspection we can write the solutions of Eqs. (10) and (11) in terms of harmonic-oscillator functions $\Phi_n$:

$$f_a=\begin{bmatrix} a_1\Phi_n \\ a_3\Phi_{n-1} \\ a_5\Phi_{n+1} \\ a_7\Phi_{n+1} \end{bmatrix},\quad f_b=\begin{bmatrix} a_2\Phi_n \\ a_6\Phi_{n-1} \\ a_4\Phi_{n+1} \\ a_8\Phi_{n-1} \end{bmatrix}. \tag{16}$$

We then obtain the following determinantal equations for the eigenvalues of the $a$ and $b$ sets:

$$\begin{vmatrix} \epsilon_g-\epsilon_a+s(n+1)+2sF(n+\frac{1}{2}) & i(sn)^{1/2}P & i[\frac{1}{3}s(n+1)]^{1/2}P & [\frac{2}{3}s(n+1)]^{1/2}P \\ -i(sn)^{1/2}P & -s[(\gamma_1+\gamma')(n-\frac{1}{2})+\frac{3}{2}\kappa]-\epsilon_a & -s[3n(n+1)]^{1/2}\gamma'' & -is[6n(n+1)]^{1/2}\gamma' \\ -i[\frac{1}{3}s(n+1)]^{1/2}P & -s[3n(n+1)]^{1/2}\gamma'' & -s[(\gamma_1-\gamma')(n+\frac{3}{2})-\frac{1}{2}\kappa]-\epsilon_a & is(2)^{1/2}[\gamma'(n+\frac{3}{2})-\frac{1}{2}\kappa] \\ [\frac{2}{3}s(n+1)]^{1/2}P & is[6n(n+1)]^{1/2}\gamma' & -is(2)^{1/2}[\gamma'(n+\frac{3}{2})-\frac{1}{2}\kappa] & -s[\gamma_1(n+\frac{3}{2})-\kappa]-\Delta-\epsilon_a \end{vmatrix}=0, \tag{17}$$

and

$$\begin{vmatrix} \epsilon_g-\epsilon_b+sn+2sF(n+\frac{1}{2}) & i(\frac{1}{3}sn)^{1/2}P & i[s(n+1)]^{1/2}P & (\frac{2}{3}sn)^{1/2}P \\ -i(\frac{1}{3}sn)^{1/2}P & -s[(\gamma_1-\gamma')(n-\frac{1}{2})+\frac{1}{2}\kappa]-\epsilon_b & -s[3n(n+1)]^{1/2}\gamma'' & is(2)^{1/2}[\gamma'(n-\frac{1}{2})+\frac{1}{2}\kappa] \\ -i[s(n+1)]^{1/2}P & -s[3n(n+1)]^{1/2}\gamma'' & -s[(\gamma_1+\gamma')(n+\frac{3}{2})-\frac{3}{2}\kappa]-\epsilon_b & is[6n(n+1)]^{1/2}\gamma' \\ (\frac{2}{3}sn)^{1/2}P & -is(2)^{1/2}[\gamma'(n-\frac{1}{2})+\frac{1}{2}\kappa] & -is[6n(n+1)]^{1/2}\gamma' & -s[\gamma_1(n-\frac{1}{2})+\kappa]-\Delta-\epsilon_b \end{vmatrix}=0. \tag{18}$$

These equations hold for $n\geq 1$. For $n=-1$ we set $a_1=a_3=a_2=a_6=a_8=0$, while for $n=0$ we set $a_3=a_6=a_8=0$. The eigenvalues and eigenvectors may now be computed numerically from Eqs. (16) to (18) for a given set of band parameters.

In the limit where $\epsilon_g\gg\Delta$ (which is not the case for InSb), we could treat the conduction band as decoupled from the valence band. Equations (17) and (18) then reduce to $3\times 3$ equations (B9) and (B10) of Roth *et al.*,[16] apart from some signs of off-diagonal

elements which differ because of the choice of phase of the basis functions. This, of course, makes no difference to the eigenvalues. Similarly, if we neglect all higher band terms (retaining the coupling between conduction and valence bands) Eq. (8) reduces to Eq. (2) of Bowers and Yafet[10] for the case of $\mathbf{k}_3=0$.

### II. Selection Rules and Transition Probabilities

As discussed in Refs. 15–17 the first-order wave functions are given in terms of the $f$'s of Eq. (1) and the band-edge functions by

$$\Psi=\sum_j f_j(\mathbf{r})u_{j,0}(\mathbf{r}) +\sum_i[(\epsilon_0-\epsilon_i)^{-1}\sum_j \boldsymbol{\pi}_{ij}\cdot\mathbf{k}f_j(\mathbf{r})]u_{i,0}(\mathbf{r}). \quad (19)$$

The matrix element for direct optical transitions between the valence and conduction bands is then given by[16]

$$\langle\Psi^I|\boldsymbol{\pi}\cdot\boldsymbol{\varepsilon}|\Psi^F\rangle=[\sum_{j,j'}\boldsymbol{\pi}_{jj'}\cdot\boldsymbol{\varepsilon}]\langle f_j{}^I|f_{j'}{}^F\rangle +\sum_{j,j'}\boldsymbol{\varepsilon}\cdot[\sum_i \boldsymbol{\pi}_{ji}\boldsymbol{\pi}_{ij'}/(\epsilon_0-\epsilon_i)+\sum_i \boldsymbol{\pi}_{ij'}\boldsymbol{\pi}_{ji}/(\epsilon_0-\epsilon_i)] \cdot\langle f_j{}^I|\mathbf{k}|f_{j'}{}^F\rangle, \quad (20)$$

where $\boldsymbol{\varepsilon}$ is a unit vector in the direction of the electric field of the incident radiation. $I$ is the initial (valence-band) state and $F$ the final (conduction-band) state. It is assumed here that the second term in Eq. (19) is small. The first term in Eq. (20) gives the allowed transitions. The second term, which is nonzero in InSb because of lack of inversion symmetry, gives rise to forbidden transitions obeying selection rules $\Delta n=\pm1$, The allowed transitions may be separated into two types. The dominant transitions ($\Delta n=0, -2$) arise from $D_0$ in Eq. (7). In addition weaker allowed transitions arise from $D_1$ in this equation. Following Luttinger[11] we include $D_1$ by second-order perturbation theory for the magnetic field in the [110] and [100] directions (these are the orientations for which the fine-structure experiments were carried out). To calculate the transition probabilities, we have taken the valence band as decoupled from the conduction band, and neglected the effect of the split-off band, since this produces negligible error here. The problem thus reduces to the solution of two (2×2) perturbation problems (Appendix A).

The strength of the dominant contributions to the magneto-absorption spectrum ($\Delta n=0, -2$) is proportional to $P^2$ and the first power of $H$, and is independent of $n$. The strength of the $D_1$-induced contributions is proportional to $P^2$, $H$, and a quantity like $Q=[s^2\mu^2(n+1)(n+2)]/(\Delta\epsilon)^2$, where $\mu=\frac{1}{2}(\gamma_3-\gamma_2)$ and $\Delta\epsilon$ is the difference between two magnetic levels in the valence band differing in quantum number by two or four. In cases where $Q$ involves two heavy-hole levels, the denominator may be small enough to yield an appreciable intensity for these transitions. Thus these contributions are predominantly from heavy-hole to conduction-band transitions.

The forbidden transition strengths are proportional to the square of the magnetic field, to $G^2$, and also to $n$ or $(n+1)$. Since $G$ is estimated to be of the order of 2, the transition strengths calculated from Eq. (20) for $H=100$ kG and $n<4$ are estimated to be less than 1% of the strength of the dominant allowed transitions. We therefore do not include them in our analysis of the experimental data.

We use the conventional notation of Luttinger for the (+) and (−) valence-band energy-level ladders. In the high-quantum limit the level spacing in these ladders tends to the cyclotron-resonance spacing of the light hole and heavy hole, respectively, so we refer to them as light-hole and heavy-hole ladders. The relative strengths of the $D_1$-induced transitions are calculated in the

TABLE I. Selection rules and relative transition probabilities for allowed ($\Delta n=0, -2$) and warping-induced transitions. The notation is a modification of that used by Roth *et al.*[16] $a$ and $b$ refer to energy levels in the $a$ and $b$ sets; +, −, and $c$ refer to the light-hole, heavy-hole, and conduction electron, respectively. The orbital quantum number is given in brackets. For $\mathbf{H}\|[110]$ the selection rules for the $D_1$-induced transitions are the same as for $\mathbf{H}\|[100]$, but the polarization properties are different, resulting in some extra transitions.

| Transition | $\sigma_L$ | | $\sigma_R$ | | $\pi$ | |
|---|---|---|---|---|---|---|
| Allowed | $\Delta n=0$ | | $\Delta n=-2$ | | ... | |
| $a^\pm(n)a^c(n')$ | $\frac{1}{3}(a_5{}^\pm)^2$ | | $(a_3{}^\pm)^2$ | | | |
| | $\Delta n=0$ | | $\Delta n=-2$ | | ... | |
| $b^\pm(n)b^c(n')$ | $(a_4{}^\pm)^2$ | | $\frac{1}{3}(a_6{}^\pm)^2$ | | | |
| | | | | | $\Delta n=0$ | |
| $a^\pm(n)b^c(n')$ | ... | | ... | | $\frac{2}{3}(a_5{}^\pm)^2$ | |
| | | | | | $\Delta n=-2$ | |
| $b^\pm(n)a^c(n')$ | ... | | ... | | $\frac{2}{3}(a_6{}^\pm)^2$ | |
| $D_1$-induced $\mathbf{H}\|[100]$ | | | | | | |
| | $\Delta n=+4$ | $\Delta n=-4$ | $\Delta n=+2$ | $\Delta n=-6$ | ... | |
| $a^\pm(n)a^c(n')$ | $\frac{1}{3}C_5{}^{\pm2}(+4)$ | $\frac{1}{3}C_5{}^{\pm2}(-4)$ | $C_3{}^{\pm2}(+4)$ | $C_5{}^{\pm2}(-4)$ | | |
| $b^\pm(n)b^c(n')$ | $C_4{}^{\pm2}(+4)$ | $C_4{}^{\pm2}(-4)$ | $\frac{1}{3}C_6{}^{\pm2}(+4)$ | $\frac{1}{3}C_6{}^{\pm2}(-4)$ | ... | |
| | | | | | $\Delta n=+4$ | $\Delta n=-4$ |
| $a^\pm(n)b^c(n')$ | ... | ... | ... | ... | $\frac{2}{3}C_5{}^{\pm2}(+4)$ | $\frac{2}{3}C_5{}^{\pm2}(-4)$ |
| | | | | | $\Delta n=+2$ | $\Delta n=-6$ |
| $b^\pm(n)a^c(n')$ | ... | ... | ... | ... | $\frac{2}{3}C_6{}^{\pm2}(+4)$ | $\frac{2}{3}C_6{}^{\pm2}(-4)$ |

Appendix for $H$ in the [110] and [100] directions. In Table I both the selection rules for the orbital quantum number and the relative transition strengths are given in the appropriate space for each polarization. We use conventional notation for left- and right-handed circular polarization. For the allowed transitions $\sigma_L$ corresponds to $\Delta M_J=+1$ and $\sigma_R$ to $\Delta M_J=-1$, where $M_J$ is the total-angular-momentum quantum number.

## EXPERIMENTAL METHOD

Conventional methods were used to obtain the magneto-absorption and Faraday rotation spectra on thin freely mounted samples of pure $n$-type InSb ($N\sim10^{14}$ cm$^{-3}$) at liquid-helium temperature. The required spectral resolution was achieved with a Perkin-Elmer double-pass grating spectrometer and cooled (77°K)PbSe and PbS detectors. The signal output was amplified with a phase-sensitive lock-in amplifier and displayed on a recorder. Samples of thickness varying from 4 to 10 $\mu$ were freely mounted in a copper "cold finger" arrangement. Since the thermal path to the liquid-helium chamber was via a piece of gold foil (attached to one end of the sample with a two-component silver solder[19]) the sample temperature was estimated to be about 20°K.

A silver chloride pile-of-plates polarizer was used to obtain plane-polarized light in the Voigt configuration, and in conjunction with a CsI Fresnel rhomb to obtain circularly polarized light in the Faraday configuration. A modification of the phase-sensitive technique described previously[20] was used to measure the Faraday rotation. The analyzer was set first at 45° with respect to the polarizer and then at 135° for a given setting of the magnetic field. The rotation $\theta$ was then obtained from the equation

$$\sin2\theta=[I(45°)-I(135°)]/[I(45°)+I(135°)], \quad (21)$$

where $I(45°)$ and $I(135°)$ are the intensities transmitted with the analyzer at 45° and 135°, respectively. The advantage of this method (which is accurate for rotations $>1$ deg) is that the wavelength can be swept continuously to obtain a complete spectrum.

The magneto-absorption data were taken both by sweeping $H$ from 0 to 96.5 kG at fixed wavelengths, and by sweeping the wavelength at selected values of $H$. The photon energy range studied was from the absorption edge at 0.235 eV to an upper limit of 0.500 eV.

## EXPERIMENTAL RESULTS

In Fig. 1 are shown plots of photon energy of the transmission minima as a function of magnetic-field strength for the principal transitions in the $\mathbf{E}\perp\mathbf{H}$ (i.e., $\sigma_L$ and $\sigma_R$) spectrum, with $\mathbf{H}$ parallel to the [100] crystal direction. The theoretical assignment (see next section) shows that apart from two transitions from heavy-hole levels, the rest of the transitions shown are from light-hole levels. In Fig. 2 are shown similar plots for the $\mathbf{E}\|\mathbf{H}$ spectrum, again for $\mathbf{H}$ parallel to the [100] direction. Here the strongest transitions are from heavy-hole levels. The nonparabolic effects of the conduction and valence bands are shown by the curvature of the lines. The solid lines are obtained theoretically as discussed in the next section.

Plots of the ratio $I(H)/I(0)$ as a function of photon energy are given in Fig. 3 for $\mathbf{E}\|\mathbf{H}$ with $H$ parallel to the [110] and [100] crystal directions. Further plots are shown in Fig. 4 for $\mathbf{E}\perp\mathbf{H}$ with left and right circularly polarized light. The magnetic field is parallel to the [100] direction in this case. Also shown in Fig. 4 is the Faraday rotation spectrum. This latter is proportional to the difference between contributions to the dispersion from $\Delta M_J=+1$ and $\Delta M_J=-1$ transitions, and should therefore show resonances near the same positions as the combined $\sigma_L$ and $\sigma_R$ spectra. In Figs. 5 and 6, the first few transitions of the $\sigma_L$, $\sigma_R$, and Faraday rotation spectra are shown in greater detail.

## NUMERICAL RESULTS AND DISCUSSION

As pointed out by Roth[16] the experimental determination of band-edge parameters from magneto-absorption spectra is considerably complicated by the fact that it is necessary to go to higher order than $k^2$ in effective-

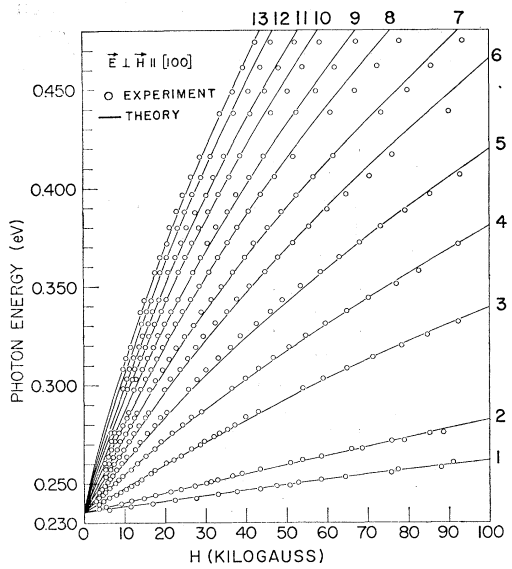


FIG. 1. Plot of the photon energy of the principal transmission minima as a function of magnetic field for $\mathbf{E}\perp\mathbf{H}$. The notation for the transitions is defined in Table I. The solid lines are obtained according to the theory of Eqs. (17) and (18). The transitions are as follows:

1. $a^-(2)a^c(0)$
2. $b^+(0)b^c(0)$
3. $a^+(1)a^c(1)$
4. $b^+(1)b^c(1)$
5. $a^+(3)a^c(1)$
6. $b^+(2)b^c(2)$
7. $a^+(4)a^c(2)$
8. $b^+(3)b^c(3)$
9. $a^+(5)a^c(3)$
10. $b^+(4)b^c(4)$
11. $b^+(6)b^c(4)$
12. $b^+(5)b^c(5)$
13. $a^+(7)a^c(5)$

[19] Q. H. F. Vrehen, Phys. Rev. **145**, 675 (1966).
[20] C. R. Pidgeon and S. D. Smith, Infrared Phys. 4, 13 (1964).

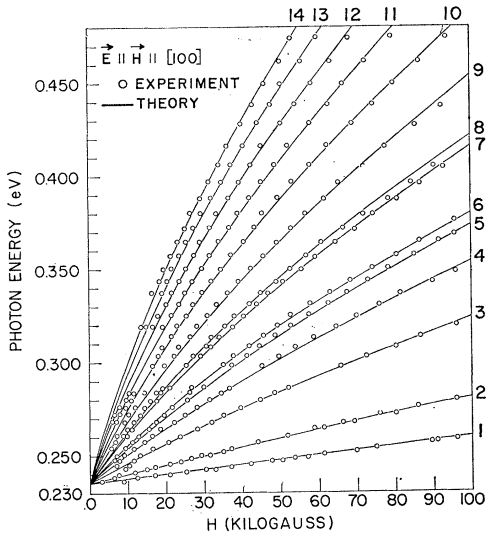


FIG. 2. Plot of the photon energy of the principal transmission minima as a function of magnetic field for **E**∥**H**. The solid lines are obtained from Eqs. (17) and (18). The transitions are given as follows:

1. $b^-(2)a^c(0)$
2. $a^+(0)b^c(0)$
3. $b^-(3)a^c(1)$
4. $a^+(1)b^c(1)$
5. $b^-(4)a^c(2)$
6. $a^-(2)b^c(2)$
7. $b^-(5)a^c(3)$
8. $a^-(3)b^c(3)$
9. $b^-(6)a^c(4)$
10. $b^-(7)a^c(5)$
11. $b^-(8)a^c(6)$
12. $b^-(9)a^c(7)$
13. $b^-(10)a^c(8)$
14. $b^-(11)a^c(9)$

mass theory for the interaction between conduction and valence bands. For this reason we have used existing cyclotron-resonance results for the conduction and valence bands of InSb to obtain a preliminary set of parameters for the assignment of the principal transi-

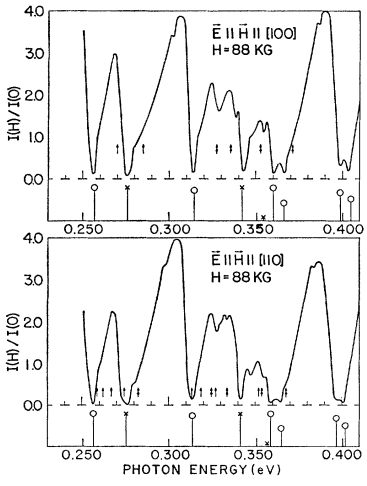


FIG. 3. Plots of the ratio of transmitted intensity with the magnetic field applied to that for zero field, $I(H)/I(0)$, against photon energy for **H**∥[100] and **H**∥[110], with **E**∥**H**. The theoretical positions and relative strengths of the allowed ($\Delta n=0, -2$) transitions are shown beneath the spectra. Crosses represent light-hole transitions, circles heavy-hole transitions. The single arrows show the positions of $D_1$-induced transitions of estimated strength $>1/30$ of that of the allowed transitions, the double arrows those of strength $>1/15$ of the allowed transitions.

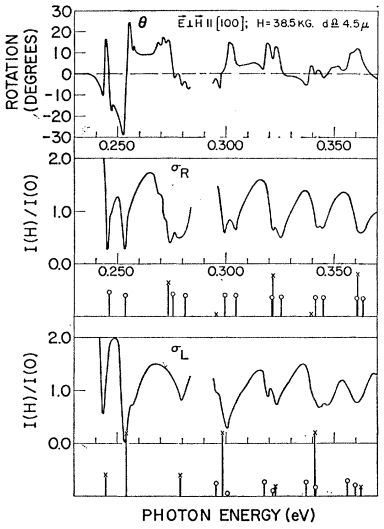


FIG. 4. Plots of Faraday rotation, and $I(H)/I(0)$ for left and right circularly polarized light, against photon energy. The theoretical positions and relative strengths of the allowed transitions are shown beneath the spectra. Crosses represent light-hole transitions, circles heavy-hole transitions.

tions. We take the following preliminary set:

$$P^2=0.39 \text{ atomic units (au)},$$
$$\Delta=0.9 \text{ eV},$$
$$F=0,$$

(Lax *et al.*, Palik *et al.*[21]; Kane[9]);

$$\gamma_1^L=25,$$
$$\gamma_2^L=10.5, \qquad (22)$$
$$\gamma_3^L=11.5,$$

(Bagguley *et al.*[7]).

$\epsilon_g$ is given from our experiments as 0.2355 eV in agreement with Zwerdling *et al.*[3] (here we have added $7\times10^{-4}$ eV for the estimated zero-field exciton binding

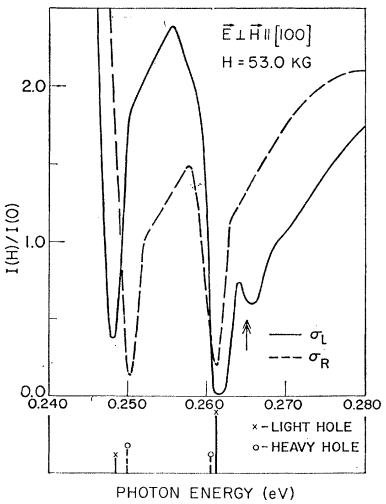


FIG. 5. Detail of the $\sigma_L$ and $\sigma_R$ magneto-absorption spectra for the first few transitions. The double-headed arrow shows the position of a $D_1$-induced transition (of strength $>\frac{1}{10}$ of that of the allowed transitions) expected theoretically and observed in the $\sigma_L$ spectrum.

[21] B. Lax, J. G. Mavroides, H. J. Zeiger, and R. J. Keyes, Phys. Rev. **122**, 31 (1961); E. D. Palik, G. S. Picus, S. Teitler, and R. F. Wallis, Phys. Rev. **122**, 475 (1961).

energy). $\kappa$ is given by the following approximate expression[22,17]

$$\kappa^L=\gamma_3{}^L+\tfrac{2}{3}\gamma_2{}^L-\tfrac{1}{3}\gamma_1{}^L-\tfrac{2}{3}. \quad (23)$$

We then use the following procedure to improve the fit and obtain a final set of band parameters. The dominant intermediate quantum number *light-hole* transitions are relatively insensitive to the higher band parameters, so that we may adjust $\Delta$ and $P^2$ for best fit for the light-hole spectra of Fig. 1. These values in conjunction with the measured energy gap give the conduction-band effective mass $m_c/m_0$, and $g$ factor $g_c$ and the light-hole mass $m_{l.h.}/m_0$ at the band edge. It is then possible to adjust the higher band parameters to obtain the best fit for the heavy-hole spectra (Fig. 2) which is at the same time consistent with the experimentally measured anisotropy (Fig. 3).

Finally we obtain the following band-edge parameters for a good over-all fit of all the spectra:

$$P^2=0.403 \text{ au},$$
$$\epsilon_g=0.2355 \text{ eV},$$
$$\Delta=0.9 \text{ eV},$$
$$\gamma_1{}^L=32.5,$$
$$\gamma_2{}^L=14.3,$$
$$\gamma_3{}^L=15.4,$$
$$\kappa^L=13.4.$$

The parameter $F$ is expected to be very small[9] and appears to have negligible effect on the levels so we put it equal to zero.

Using these parameters the solid lines obtained from the theory of the previous sections are shown in Figs. 1 and 2 for the principal light- and heavy-hole transitions. It is seen that the plots of photon energy of absorption maxima versus magnetic field rapidly depart from linearity above $H=10$ kG, showing very clearly the effects of nonparabolicity of the conduction and valence bands. The over-all fit for heavy-hole → electron transitions is extremely good; but that for the light-hole → electron transitions is not quite as good, which would seem to imply that the light hole is more nonparabolic than given by this theory. This may mean that to get a better fit, one would have to include the $\Gamma_{15}$ band (the first higher band above the conduction band) to higher order than $k^2$ in the theory.

In Fig. 3 we show the relative strengths and positions (calculated according to Table I) of all the ($\Delta n=0, -2$) allowed transitions for $\mathbf{E}\|\mathbf{H}$, with $\mathbf{H}\|[100]$ and $[110]$. Two features are immediately obvious from the experimental spectra. Firstly the anisotropy is small, and although in quite good agreement with the theoretical predictions ($\gamma_3-\gamma_2=1.1$) cannot be used by itself to obtain an accurate determination of band parameters

[22] G. Dresselhaus, A. F. Kip, and C. Kittel, Phys. Rev. 98, 368 (1955).

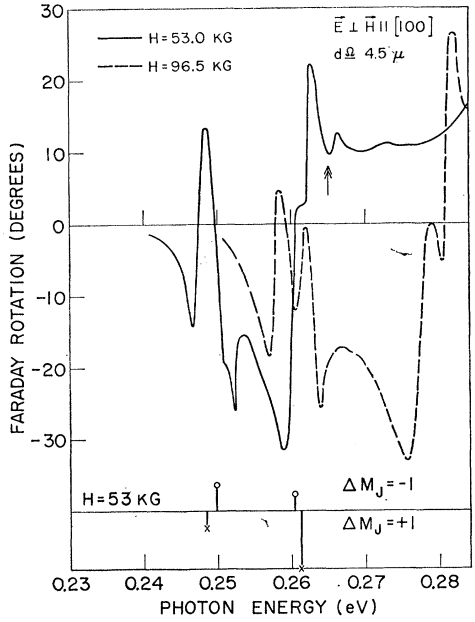


FIG. 6. Detail of the Faraday rotation spectrum for the first few transitions. The strong $D_1$-induced transition indicated in Fig. 5 also shows up in Faraday rotation (double-headed arrow) as a characteristic dispersion shape.

$\gamma_1{}^L$, $\gamma_2{}^L$, $\gamma_3{}^L$, and $\kappa^L$. Table II shows the theoretical and experimental anisotropies for the $\Delta n=0, -2$ transitions of Fig. 3. A feature which is predicted by the theory is that the anisotropy of the heavy hole and electron go the same way, and therefore reinforce. However, the light-hole anisotropy is of opposite sign so that for the light-hole → electron transitions the anisotropy may cancel or appear to go the wrong way. This has been observed experimentally. Secondly, there is more structure in the spectra than can be accounted for purely in terms of allowed transitions ($\Delta n=0, -2$). It appears that some of the additional structure both for $\mathbf{H}\|[100]$ and $\mathbf{H}\|[110]$ correlates quite well with the $D_1$-induced transitions whose positions are shown by the arrows in Fig. 3.

In Fig. 4 the main structure in the $\sigma_L$ and $\sigma_R$ spectra observed for $H=38.5$ kG is associated with the $\Delta n=0, -2$ light-hole-to-electron transitions as shown. How-

TABLE II. Comparison of experiment with theory for anisotropy of transitions in $\pi$ spectrum.

| Transition | $E[100]-E[110]$ (meV) Theory | Experiment |
|---|---|---|
| $b^-(2)a^c(0)$ | 0.5 | 0 |
| $a^+(0)b^c(0)$ | 0.5 | 0 |
| $b^-(3)a^c(1)$ | 1.0 | 0.5 |
| $a^+(1)b^c(1)$ | 1.0 | 1.0 |
| $b^+(2)a^c(0)$ | −1.5 | −1.0 |
| $b^-(4)a^c(2)$ | 1.5 | 1.5 |
| $a^-(2)b^c(2)$ | 1.5 | 1.5 |
| $b^-(5)a^c(3)$ | 2.0 | 2.0 |
| $a^-(3)b^c(3)$ | 3.0 | 2.5 |

ever, at the high fields a strong feature appears on the high-energy side of the second main minimum of the $\sigma_L$ spectrum (Fig. 5) which again correlates with the strong $D_1$-induced transition marked by a double arrow. This is demonstrated by a characteristic feature in the Faraday rotation spectra in Fig. 6.

Additional fine structure might result from **H** not being exactly parallel to the principal crystal directions. It is also possible that the approximate estimate[10] for $G$ is too low, in which case forbidden transitions might be observable at the highest fields used.

It is thought on theoretical grounds (see Elliott and Loudon[23]) that the transitions involved in magneto-absorption experiments should properly be considered as being to exciton levels as opposed to being between Landau levels of the conduction and valence bands. Unfortunately there is no adequate exciton theory for the case of complex coupled energy bands. Our approach has therefore been to treat the Landau-level theory as accurately as possible and look for differences between the calculated and observed energies for the lowest transitions where exciton effects should be most important. In fact as seen in Fig. 2 we get a good over-all fit, to 2 or 3 meV at highest fields, by an appropriate choice of band parameters. We feel that this provides indirect evidence on the upper limit of the exciton binding energies at these fields.

## CONCLUSION

Measurement of magneto-absorption spectra in InSb gives the energy gap directly. However, the other band parameters may be derived only by calculation and computation involving an over-all fit of all the spectra. The energy gap obtained from the present work ($\epsilon_g=0.2355\pm0.0005$ eV) is in good agreement with that of Zwerdling *et al.*[3] We deduce the following values of effective mass for $T\sim20°$K: $m_c=0.0145\ m_0$; $m_{l.h.}=0.0160\ m_0$; $m_{h.h.}[111]=0.44\ m_0$; $m_{h.h.}[110]=0.42\ m_0$; $m_{h.h.}[100]=0.32\ m_0$; and the conduction-band $g$ factor $=-48$. The conduction-band mass and $g$ factor are in good agreement with the results of Zwerdling *et al.*[3] The valence-band masses and the anisotropy of the heavy-hole mass agree well with the cyclotron-resonance measurements of Bagguley *et al.* on $p$-type InSb,[7] the heavy mass being approximately twice the preliminary value given by Zwerdling *et al.* We wish to emphasize, however, that small changes in the parameters $\gamma_1^L$, $\gamma_2^L$, and $\gamma_3^L$ produce large changes in the deduced heavy mass so that this latter cannot be determined accurately from magneto-absorption measurements. We estimate the error in the conduction-band and light-hole masses to be about 4%.

## ACKNOWLEDGMENTS

The authors are grateful to Professor B. Lax for his support and encouragement throughout this work, to Dr. Q. Vrehen and Dr. S. Groves for helpful discussions and a careful reading of the manuscript, to Mrs. Ruth Sheshinsky for numerical computations, and to Dr. G. Dresselhaus for suggestions concerning interpretation of the observed fine structure.

We would like to thank J. Casteris for help with the construction of apparatus, and W. Tice for careful preparation of thin samples.

## APPENDIX: PERTURBATION THEORY FOR $D_1$

We treat the cases of $H$ in the [100] and [110] directions since the experiments are carried out for these orientations. In the decoupled scheme, then, $D_0$ and $D_1$ are given by

$$D_0=\begin{bmatrix} D_a' & 0 \\ 0 & D_b' \end{bmatrix}, \tag{A1}$$

$$D_1=\begin{bmatrix} D_{1,a}' & 0 \\ 0 & D_{1,b}' \end{bmatrix}, \tag{A2}$$

where

$$D_a'=-s\begin{bmatrix} [(\gamma_1^L+\gamma^{L'})(N+\frac{1}{2})+\frac{3}{2}\kappa^L] & \sqrt{3}\gamma^{L''}a^2 \\ \sqrt{3}\gamma^{L''}a^{\dagger 2} & [(\gamma_1^L-\gamma^{L'})(N+\frac{1}{2})-\frac{1}{2}\kappa^L] \end{bmatrix}, \tag{A3}$$

$$D_b'=-s\begin{bmatrix} [(\gamma_1^L-\gamma^{L'})(N+\frac{1}{2})+\frac{1}{2}\kappa^L] & \sqrt{3}\gamma^{L''}a^2 \\ \sqrt{3}\gamma^{L''}a^{\dagger 2} & [(\gamma_1^L+\gamma^{L'})(N+\frac{1}{2})-\frac{3}{2}\kappa^L] \end{bmatrix}. \tag{A4}$$

$\gamma^{L'}$ and $\gamma^{L''}$ are defined as in Eq. (13). For the [110] and [100] directions:

$$D_{1,a}'=\frac{s\sqrt{3}\mu}{2}\begin{bmatrix} r_1 & r_2 \\ r_2^\dagger & -r_1 \end{bmatrix};\quad D_{1,b}'=\frac{s\sqrt{3}\mu}{2}\begin{bmatrix} -r_1 & r_2 \\ r_2^\dagger & r_1 \end{bmatrix}, \tag{A5}$$

where

$$\begin{aligned} r_1&=\tfrac{1}{2}\sqrt{3}\sin^2\theta(3\cos^2\theta-1)(a^2+a^{\dagger 2}),\\ r_2&=(3\cos^2\theta-1)[\tfrac{1}{2}(\cos^2\theta-3)a^{\dagger 2}-\sin^2\theta(N+\tfrac{1}{2})],\\ \mu&=\tfrac{1}{2}(\gamma_3-\gamma_2). \end{aligned} \tag{A6}$$

The perturbed functions in the $a$ set are solutions of the equation

$$(D_a'+D_{1,a}')\bar{f}_{a,n}=\epsilon_{a,n}\bar{f}_{a,n}, \tag{A7}$$

[23] R. J. Elliott and R. Loudon, J. Phys. Chem. Solids **15**, 196 (1960).

and are given by

$$\bar{f}_{a,n^s}=N_{a,n^s}(f_{a,n^s}+\sum_{n'\neq n,t} A_{n,n'^{s,t}}f_{a,n'^t}), \quad \text{(A8)}$$

where $s$ and $t$ run over the light-hole (+) and heavy-hole (−) levels, $N_n$ is a normalization factor, and

$$A_{n,n'^{s,t}}=\langle f_{a,n'^t}|D_{1,a}'|f_{a,n^s}\rangle/(\epsilon_{a,n^s}-\epsilon_{a,n'^t}). \quad \text{(A9)}$$

We have similar equations for the $b$ set. Working in the uncoupled scheme the unperturbed valence-band functions are

$$f_{a,n^\pm}=\begin{pmatrix} a_{3,n^\pm} & \Phi_{n-2} \\ a_{5,n^\pm} & \Phi_n \end{pmatrix}; \quad f_{b,n^\pm}=\begin{pmatrix} a_{6,n^\pm} & \Phi_{n-2} \\ a_{4,n^\pm} & \Phi_n \end{pmatrix}. \quad \text{(A10)}$$

We first consider the [100] case, giving for the $a$ set

$$\langle f_{a,n'^t}|D_{b,a}'|f_{a,n^s}\rangle = s\sqrt{3}\mu\{a_{3,n'^\pm}a_{5,n^s}[(n+1)(n+2)]^{1/2}\delta_{n+4,n'} + a_{5,n'^t}a_{3,n^s}[(n-2)(n-3)]^{1/2}\delta_{n-4,n'}\}. \quad \text{(A11)}$$

For the $b$ set

$$\langle f_{b,n'^t}|D_{1,b}'|f_{b,n^s}\rangle = s\sqrt{3}\mu\{a_{6,n'^t}a_{4,n^s}[(n+1)(n+2)]^{1/2}\delta_{n+4,n'} + a_{4,n'^t}a_{6,n^s}[(n-2)(n-3)]^{1/2}\delta_{n-4,n'}\}. \quad \text{(A12)}$$

We now consider the four classes of valence-to-conduction-band transitions $a\rightarrow a$, $b\rightarrow b$, $a\rightarrow b$, and $b\rightarrow a$. For the transition probability we evaluate matrix elements of type $\langle\bar{\Psi}_{n^\pm}|\boldsymbol{\pi}\cdot\boldsymbol{\varepsilon}|\Psi_{n'^c}\rangle$, where the perturbed valence-band functions are

$$\bar{\Psi}_{a,n^\pm}=\bar{f}_{3,n^\pm}u_{3,0}(\mathbf{r})+\bar{f}_{5,n^\pm}u_{5,0}(\mathbf{r}), \quad \text{(A13)}$$

$$\bar{\Psi}_{b,n^\pm}=\bar{f}_{6,n^\pm}u_{6,0}(\mathbf{r})+\bar{f}_{4,n^\pm}u_{4,0}(\mathbf{r}). \quad \text{(A14)}$$

The unperturbed conduction-band functions are

$$\Psi_{a,n'^c}=\Phi_{n'}u_{1,0}(\mathbf{r})$$

and

$$\Psi_{b,n'^c}=\Phi_{n'}u_{2,0}(\mathbf{r}). \quad \text{(A15)}$$

Then for the $a\rightarrow a$ transition probability ($H\|[100]$):

$$\langle\bar{\Psi}_{a,n^\pm}|\boldsymbol{\pi}\cdot\boldsymbol{\varepsilon}|\Psi_{a,n'^c}\rangle=\sum_t N_{a,n^\pm}\{[a_{3,n^\pm}\delta_{n-2,n'}+A_{n,n+4^{\pm,t}}a_{3,n+4^t}\delta_{n+2,n'}+A_{n,n-4^{\pm,t}}a_{3,n-4^t}\delta_{n-6,n'}](\boldsymbol{\pi}_{3,1}\cdot\boldsymbol{\varepsilon}) + [a_{5,n^\pm}\delta_{n,n'}+A_{n,n+4^{\pm,t}}a_{5,n+4^t}\delta_{n+4,n'}+A_{n,n-4^{\pm,t}}a_{5,n-4^t}\delta_{n-4,n'}](\boldsymbol{\pi}_{5,1}\cdot\boldsymbol{\varepsilon})\}. \quad \text{(A16)}$$

We define constants $C_3^\pm(\pm4)$ and $C_5^\pm(\pm4)$ by

$$\langle\bar{\Psi}_{a,n^\pm}|\boldsymbol{\pi}\cdot\boldsymbol{\varepsilon}|\Psi_{a,n'^c}\rangle=N_{a,n^\pm}[a_{3,n^\pm}\delta_{n-2,n'}+C_3^\pm(+4)\delta_{n+2,n'}+C_3^\pm(-4)\delta_{n-6,n'}](\boldsymbol{\pi}_{3,1}\cdot\boldsymbol{\varepsilon}) + N_{a,n^\pm}[a_{5,n^\pm}\delta_{n,n'}+C_5^\pm(+4)\delta_{n+4,n'}+C_5^\pm(-4)\delta_{n-4,n'}](\boldsymbol{\pi}_{5,1}\cdot\boldsymbol{\varepsilon}). \quad \text{(A17)}$$

Then we obtain similar expressions for the other transition probabilities:

$$\langle\bar{\Psi}_{a,n^\pm}|\boldsymbol{\pi}\cdot\boldsymbol{\varepsilon}|\Psi_{b,n'^c}\rangle=N_{a,n^\pm}[a_{5,n^\pm}\delta_{n,n'}+C_5^\pm(+4)\delta_{n+4,n'}+C_5^\pm(-4)\delta_{n-4,n'}](\boldsymbol{\pi}_{5,2}\cdot\boldsymbol{\varepsilon}), \quad \text{(A18)}$$

$$\langle\bar{\Psi}_{b,n^\pm}|\boldsymbol{\pi}\cdot\boldsymbol{\varepsilon}|\Psi_{a,n'^c}\rangle=N_{b,n^\pm}[a_{6,n^\pm}\delta_{n-2,n'}+C_6^\pm(+4)\delta_{n+2,n'}+C_6^\pm(-4)\delta_{n-6,n'}](\boldsymbol{\pi}_{6,1}\cdot\boldsymbol{\varepsilon}), \quad \text{(A19)}$$

$$\langle\bar{\Psi}_{b,n^\pm}|\boldsymbol{\pi}\cdot\boldsymbol{\varepsilon}|\Psi_{b,n'^c}\rangle=N_{b,n^\pm}[a_{6,n^\pm}\delta_{n-2,n'}+C_6^\pm(+4)\delta_{n+2,n'}+C_6^\pm(-4)\delta_{n-6,n'}](\boldsymbol{\pi}_{6,2}\cdot\boldsymbol{\varepsilon}) + N_{b,n^\pm}[a_{4,n^\pm}\delta_{n,n'}+C_4^\pm(+4)\delta_{n+4,n'}+C_4^\pm(-4)\delta_{n-4,n'}](\boldsymbol{\pi}_{4,2}\cdot\boldsymbol{\varepsilon}), \quad \text{(A20)}$$

where $C_6^\pm(\pm4)$ and $C_4^\pm(\pm4)$ are defined in the same way as $C_3^\pm(\pm4)$ and $C_5^\pm(\pm4)$, respectively. From Eqs. (A17) to (A20), we obtain the selection rules and transition probabilities outlined in Table I.

Similarly we calculate the transition probabilities for $H$ in the [110] direction. In this case the perturbation $D_1'$ couples magnetic levels in the valence band differing in quantum number by $\pm2$ as well as $\pm4$, which gives expressions of the following type for the transition probability:

$$\langle\bar{\Psi}_{a,n^\pm}|\boldsymbol{\pi}\cdot\boldsymbol{\varepsilon}|\Psi_{a,n'^c}\rangle = N_{a,n^\pm}[a_{3,n^\pm}\delta_{n-2,n'}+C_3^\pm(+4)\delta_{n+2,n'}+C_3^\pm(-4)\delta_{n-6,n'}+C_3^\pm(+2)\delta_{n,n'}+C_3^\pm(-2)\delta_{n-4,n'}](\boldsymbol{\pi}_{3,1}\cdot\boldsymbol{\varepsilon}) + N_{a,n^\pm}[a_{5,n^\pm}\delta_{n,n'}+C_5^\pm(+4)\delta_{n+4,n'}+C_5^\pm(-4)\delta_{n-4,n'}+C_5^\pm(+2)\delta_{n+2,n'}+C_5^\pm(-2)\delta_{n-2,n'}](\boldsymbol{\pi}_{5,1}\cdot\boldsymbol{\varepsilon}), \quad \text{(A21)}$$

where $C(\pm2)$ is defined in the same way as $C(\pm4)$. The selection rules are the same but the polarization properties slightly different for the [100] and [110] cases. For spectra in the $\sigma$ and $\pi$ configurations this results in different transition strengths and some additional transitions in the [110] case.